Al_3Sc thin films for advanced interconnect applications

Jean-Philippe Soulié,[a,*] Kiroubanand Sankaran,[a] Valeria Founta, [b,c,a] Karl Opsomer,[a] Christophe Detavernier,[d] Joris Van de Vondel,[c] Geoffrey Pourtois,[a,e] Zsolt Tőkei,[a] Johan Swerts,[a] and Christoph Adelmann,[a]

[a] Imec, 3001 Leuven, Belgium

[b] KU Leuven, Department of Materials Engineering, SCALINT, 3001 Leuven, Belgium

[c] Department of Physics and Astronomy, Quantum Solid-State Physics, 3001 Leuven, Belgium

[d] Ghent University, Department of Solid State Sciences, COCOON, 9000 Gent, Belgium

[e] Department of Chemistry, Plasmant Research Group, University of Antwerp, 2610 Wilrijk, Belgium

* Corresponding author. Email: jean-philippe.soulie@imec.be

ABSTRACT

Al_xSc_{1-x} thin films have been studied with compositions around Al_3Sc (x = 0.75) for potential interconnect metallization applications. As-deposited 25 nm films were x-ray amorphous but crystallized at 190°C with a recrystallization observed at 440°C. After annealing at 500°C, 24 nm thick stoichiometric Al_3Sc showed a resistivity of 12.6 μΩcm, limited by a combination of grain boundary and point defect (disorder) scattering. Together with *ab initio* calculations that found a mean free path of the charge carriers of 7 nm for stoichiometric Al_3Sc, these results indicate that Al_3Sc bears promise for future interconnect metallization schemes. Challenges remain in minimizing the formation of secondary phases as well as in the control of the non-stoichiometric surface oxidation and interfacial reaction with the underlying dielectrics.

KEYWORDS

Alternative metal, intermetallic, thin film, interconnect

INTRODUCTION

Today, Cu-based interconnects are progressively limiting the performance of large-scale integrated microelectronic circuits due the strongly increasing line and via resistance as well as reduced reliability.[1–4] The resistance increase originates from the ever reduction of the cross-sectional area of scaled interconnects but also from the rapidly growing Cu resistivity at nanoscale dimensions. The increasing resistivity is due to a long mean free path (MFP) of the charge carriers in Cu (of around 40 nm) that renders Cu very sensitive to finite size effects.[2,4–6] Moreover, Cu requires barrier and liner layers to ensure reliable interconnect operation, which further reduce the Cu cross-sectional area without contributing (much) to the line or via conductance, therefore further aggravating the resistance issue.

For this reason, alternatives to Cu metallization have been intensively researched in recent years.[1,4,7,8] A particular focus has been on elemental metals with short MFPs and high melting temperatures, such as Co,[9,10] which has been introduced into commercial circuits recently,[11] as well as Pt-group metals,[12] especially Ru,[13–15] or Mo.[16] Lately, the search for alternative metals has been broadened to include also binary and ternary intermetallics.[17–19] Several intermetallic aluminides,[20–22] in particular NiAl,[23–25] have been proposed and studied as potential interconnect metals. However, an ultralow resistivity at small dimensions has not been demonstrated for these aluminides yet and the search for additional binary intermetallics continues. Here, we discuss the suitability of the binary aluminide Al_3Sc as an interconnect metal candidate,[22] based on a combination of thin film studies as well as first-principles simulations of its electronic structure. Al_3Sc combines a low bulk resistivity (7 μΩcm)[26] with a high melting point (1320°C),[27] higher than that of Cu (1085°C), which can be used as a proxy for interconnect reliability. In this work, we demonstrate a low resistivity of 12.6 μΩcm for films as thin as 24 nm. We further discuss the effect of stoichiometry as well as surface oxidation on the properties of the films.

METHODOLOGY

All Al_xSc_{1-x} films have been deposited by physical vapor deposition (PVD) on 300 mm Si (100) wafers. Prior to PVD, a 100 nm thick thermal SiO_2 was grown to provide electrical insulation. PVD was performed by co-sputtering from Al and Sc targets at room temperature. A post-deposition annealing step was performed in H_2 for 30 min at atmospheric pressure. The crystal structure and the thicknesses of the films were determined by grazing-incidence x-ray diffraction (GIXRD, $\omega = 0.3°$) and x-ray reflectance (XRR), respectively, in a Bruker JVX7300 diffractometer using Cu Kα radiation. *In-situ* XRD (IS-XRD) measurements ($2\theta\text{–}\omega$ configuration) during ramp annealing were performed in a custom-built system using a Cu Kα radiation and a Bruker VANTEC detector at a heating rate of 0.2 K/s in 5%H_2/He. Additional information about crystallinity, thickness, chemical composition of the films were obtained by transmission electron microscopy (TEM) using a FEI Titan electron microscope operating at 200 kV. The resistivity of the films was determined by measuring the sheet resistance (Rs) using a KLA Tencor RS100 system in combination with the XRR film thickness, corrected for the thickness of the surface oxide, which was assumed to be insulating. Atomic force microscopy (AFM) was performed on a Bruker ICON microscope in tapping mode. The resistivity at cryogenic temperatures was obtained in a Quantum Design Physical Property Measurement System using patterned Hall bars.

The electronic properties of Al_3Sc were determined through first-principles density-functional theory (DFT) simulations. These simulations were performed using the QUANTUM ESPRESSO package, and the valence electron shells of the elements were represented by Garrity–Bennett–Rabe–Vanderbilt (GBRV) pseudopotentials[28], with a kinetic cutoff energy of 60 Ry for the truncation of the planewave expansion of the wavefunction. The exchange-correlation energy was described within the Perdew–Burke–Ernzerhof generalized gradient approximation[30]. The first Brillouin zone was sampled using a discretized Monkhorst–Pack scheme[31] based on a regular unshifted (Γ-point centered) k-point mesh of 40×40×40. These ensure a convergence of the total energy within 10^{-12} eV.

RESULTS AND DISCUSSION

Figure 1a shows the GIXRD patterns of 24.1 ± 1.1 nm thick as-deposited Al_xSc_{1-x} films as a function of the Al mole fraction x around stoichiometric Al_3Sc ($x = 0.75$). The patterns indicate that all films were amorphous within the limit of detection of our x-ray measurements. *In situ* XRD during ramp annealing (Fig. 1b) of stoichiometric a 25.0 nm thick Al_3Sc film reveals that the films show weak crystallization at 193°C, followed by recrystallization at 443°C (see Fig. 1c). The GIXRD patterns of the 24.1 ± 1.1 nm thick Al_xSc_{1-x} after post-deposition annealing at 500°C in H_2 in Fig. 1d are consistent with the $L1_2$ crystal structure (space group $Pm\bar{3}m$) of Al_3Sc.[26,27] A comparison with corresponding 2θ-ω XRD pattern (not shown) indicated that the films were polycrystalline with random grain orientation and no signs of texture. The lattice parameters extracted from the GIXRD pattern showed a linear decrease with increasing Al content (Fig. 1e). For stoichiometric Al_3Sc ($x = 0.75$), it was consistent with the bulk value of 4.10 Å[26,27] within experimental accuracy. After annealing, the Scherrer grain size for the 24.1 ± 1.1 nm thick films deduced from the GIXRD pattern was around 15 nm for stoichiometric Al_3Sc ($x = 0.75$) as well as Al-rich Al_xSc_{1-x} ($x > 0.75$) and reduced gradually to about 10 nm for Sc-rich Al_xSc_{1-x} ($x < 0.75$), as shown in Fig. 1f.

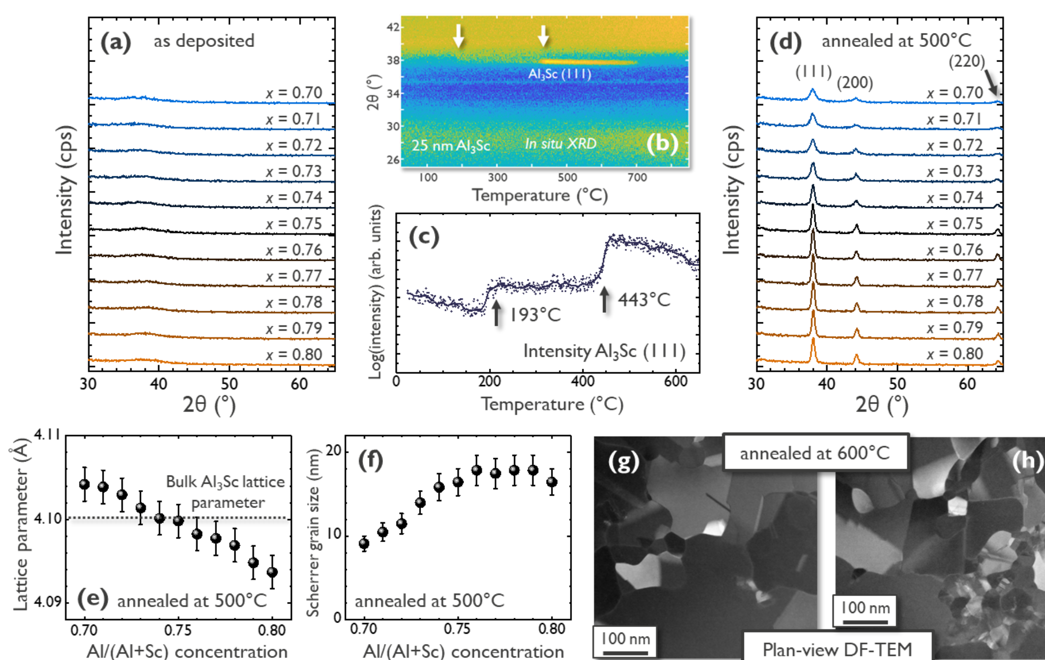

Figure 1. (a) GIXRD pattern of 24.1 ± 1.1 nm thick Al_xSc_{1-x} films deposited at room temperature as a function of Al mole fraction x. **(b)** IS-XRD pattern during ramp annealing for a 25.0 nm thick Al_3Sc (x = 0.75) film. The intensity of the Al_3Sc (111) in **(c)** shows crystallization and recrystallization at 193°C and 443°C, respectively. **(d)** GIXRD pattern of 24.1 ± 1.1 nm thick Al_xSc_{1-x} films as a function of Al mole fraction x after post-deposition annealing at 500°C. **(e)** Lattice parameter deduced from (d) as a function of Al mole fraction x. The lattice parameter of the Al_3Sc (x = 0.75) film is close to the reported bulk lattice parameter.[26,27] **(f)** Scherrer grain size deduced from (d) as a function of Al mole fraction x. **(g)** and **(h)** show plan-view dark-field (DF) TEM images of a 30 nm thick Al_3Sc film.

The crystalline nature of the annealed Al_3Sc films was confirmed by the plan-view transmission electron micrographs in Figs. 1g and 1h, both taken after annealing at 600°C in H_2. The images show a coexistence of large grains with sizes above 100 nm with zones of much smaller grains. This hints towards partial recrystallization with zones of immobile grain boundaries that have not yet moved and/or recrystallized. In these zones, the grain size is in reasonable agreement with the Scherrer grain size deduced from the GIXRD measurements.

Figure 2a shows the composition dependence of the resistivity of 24.1 ± 1.1 nm thick Al_xSc_{1-x} films as a function of their composition. As deposited films show resistivities on the order of 100 μΩcm with little dependence on composition, which is consistent with x-ray amorphous random alloys. However, the film crystallization induced by post-deposition annealing strongly reduced the resistivity with a resistivity minimum appearing for the stoichiometric Al_3Sc (x = 0.75) film. This behavior is reminiscent of that of NiAl[23,25] and can be attributed to a combination of crystallization (*cf.* Fig. 1) and possibly $L1_2$ ordering. It should be mentioned that the degree of $L1_2$ ordering is difficult to extract from XRD data since the difference with random fcc XRD patterns is very small. Hence, additional measurements are required to establish the contribution of intermetallic ordering to the thin film resistivity.

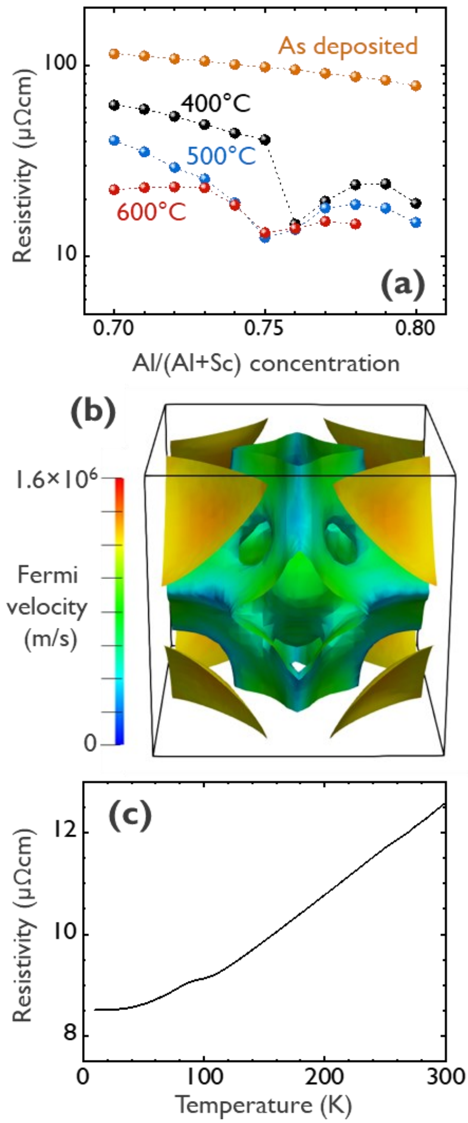

Figure 2. (a) Resistivity of 24.1 ± 1.1 nm thick Al_xSc_{1-x} films as a function of Al mole fraction *x* both as deposited and after post-deposition annealing at the indicated temperatures. **(b)** Calculated Fermi surface of $L1_2$ Al_3Sc. The color represents the intensity of the Fermi velocity. **(c)** Resistivity *vs.* temperature of a 25.0 nm thick Al_3Sc film after annealing at 500°C.

The minimum resistivity was found for the stoichiometric Al_3Sc film with a resistivity of 12.6 μΩcm after annealing at 500°C and above. This can be compared to NiAl, for which the resistivity of much thicker films (10 μΩcm at 260 nm,[23] 13 μΩcm at 56 nm[22,25]) was comparable. At similar thicknesses around 20 nm, the Al_3Sc resistivity was considerably lower than that of NiAl, which

showed a resistivity of 20.2 μΩcm for a 25.1 nm film under the same PDA conditions.[25] As discussed above, the sensitivity of the resistivity to finite size effects is governed by the MFP of the metal. The MFP (λ) of metals has been determined from both the empirical values of bulk resistivity (ρ_0) and the product of the ρ_0 and MFP($\rho_0 \times \lambda$) obtained from DFT which within a semiclassical transport framework depends on the Fermi surface morphology only.[5,32] Using a numerical integration scheme applied to the Fermi surface of Al_3Sc (see in Fig. 2b) and the procedure detailed in Refs. 5,12,32, the calculated $\rho_0 \times \lambda$ product within the constant-λ approximation[5,32] is 4.9×10^{-16} Ωm^2, i.e. very similar to that of NiAl (4.4×10^{-16} Ωm^2) and Ru (5.1×10^{-16} Ωm^2), and considerably lower than that of Cu (6.8×10^{-16} Ωm^2).[5,12] Using the reported value for the bulk resistivity of 7 μΩcm,[26] this leads to a MFP for Al_3Sc of about 7 nm, i.e. a value much shorter than that the Cu MFP of 40 nm. The above results thus indicate promising for Al_3Sc for future low-resistance scaled interconnects metallization in advanced microelectronic technology nodes, since it combines low bulk resistivity with an ultrashort MFP.

To gain further insight into the transport properties of Al_3Sc thin films, we have measured the temperature dependence of their resistivity (Fig. 2c). The resistivity increased nearly linearly with temperature over a large range, which indicates that transport was mainly limited by phonon scattering. The deviation from linearity around 80 K is not yet understood but may be linked to the phonon structure.[33] The residual resistance ratio, RRR = ρ_{300K}/ρ_{10K} was 1.5, much lower than the value of 7 observed for bulk samples.[26] This suggests a strong contribution by temperature-independent grain boundary scattering to the resistivity, which then reduces the RRR. In addition, residual disorder (point defects) also leads to temperature-independent scattering and a reduction of the RRR. A separation of the two contributions is however not possible without a detailed knowledge about the nature of the defects present in Al_3Sc, their density, and their scattering rates. A rule of thumb previously applied to other intermetallic aluminides[34] suggests that the disorder of the $L1_2$ structure in our films could be on the order of 1% assuming that the reduction of the RRR is attributed to disorder effects alone.

To further study the structure of the films, we measured the rms surface roughness of 24.1 ± 1.1 nm thick Al_xSc_{1-x} films by AFM as a function of their composition. The results in Fig 3a show low rms roughnesses below 1 nm, except for the most Al-rich Al_xSc_{1-x} films with $x \geq 0.79$. For these Al-rich films, the surface roughness is as large as 10 nm and can be attributed to large-scale up to 100 nm high dendrite-like structures (Figs. 3b and 3c). This is consistent with the occurrence of large Al clusters, in agreement with the Al-Sc phase diagram[27] (Fig. 3d) that indicates that Al_3Sc is a line compound with negligible miscibility of Al or Sc in the intermetallic.

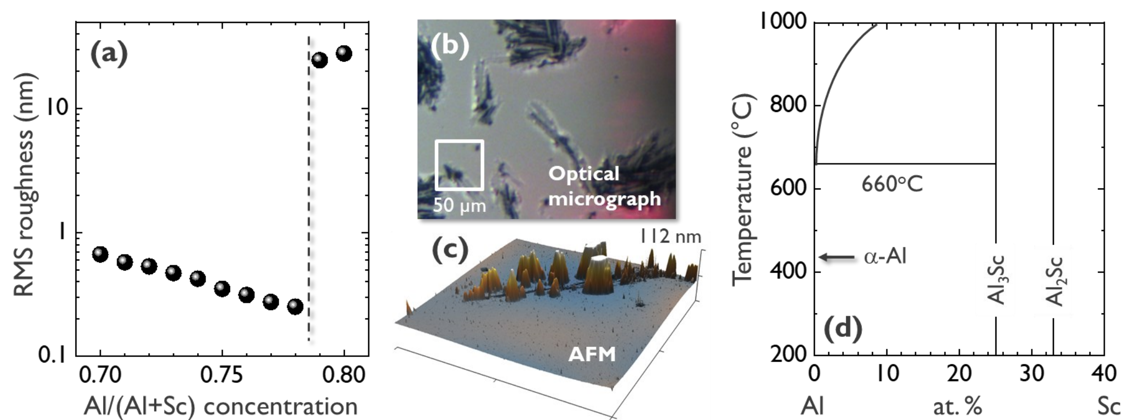

Figure 3. (a) RMS roughness of 24.1 ± 1.1 nm thick Al_xSc_{1-x} films as a function of Al mole fraction x, deduced from AFM images. **(b)** Optical micrograph and **(c)** 5 µm × 5 µm AFM topography image of the most Al-rich $Al_{0.80}Sc_{0.20}$ film. **(d)** Al-rich section of the Al-Sc phase diagram (redrawn from Ref. 27).

Hence, excess Al (or Sc) should lead to phase separation and secondary phase formation. Our experiments show that the formation of a secondary Al phase becomes visible for the studied thermal budgets in thin films in form of large dendrite-like structures around 4% of excess Al. Nonetheless, it is possible that some limited Al secondary phase, with a concentration below the AFM detection limit, is already present for less Al excess. The presence of a low-resistivity Al secondary phase may also explain the decrease of the resistivity of the most Al-rich Al_xSc_{1-x} films with $x \geq 0.79$ (Fig. 3a) after annealing. By contrast, the phase separation expected in case of an excess of Sc into Al_2Sc is not clearly observable in the data, possibly due to a much smaller length

scale for phase separation that renders the expected Al_2Sc clusters difficult to detect. We note that this behavior is markedly different from that of NiAl, which has been previously studied for interconnect applications[23-25] and possesses an extended phase field with considerable solubility of excess Ni or Al.

The polycrystalline microstructure of stoichiometric Al_3Sc films after annealing at 600°C was further confirmed by cross-sectional TEM imaging. The micrograph in Fig. 4a is consistent with the plan-view TEM images in Fig. 1g and 1h, showing the coexistence of large and small grains, separated by typically inclined ($\theta \sim 72°$) bamboo-like grain boundaries. The high-angle annular dark field (HAADF) image in Fig. 4b shows that the composition of the film is uniform.

The images further show the presence of both a ~6 nm thick surface oxide (due to air exposure between deposition and annealing) and an about 4 nm thick interfacial layer in contact with the underlying SiO_2. Chemical profiling using electron-dispersive spectroscopy (Fig. 4c) indicates that the surface oxide is non-stoichiometric (Sc-rich) with Al/Sc ~ 2, while the ratio was consistent with the expected value of 3 (within experimental precision) in the bulk part of the film. This suggests that the surface oxidation is limited by metal out-diffusion rather than O in-diffusion, with Sc diffusing faster to the surface than Al. We note that the detection of low O levels in the bulk part of the Al_3Sc film may stem from the sample preparation or measurement artifacts since XPS profiling (not shown) found O levels to be on the order of the background of 1 at.%. Finally, the chemical profile also shows that annealing at 600°C leads to a reaction with the underlying SiO_2, forming an inhomogeneous $AlScSiO_x$/$AlScO_y$ layer. This may indicate that the interface formation of Al_3Sc on low-k dielectrics requires further study and could necessitate the introduction of dielectric barrier layers or the optimization of the thermal budget for their interconnect integration.

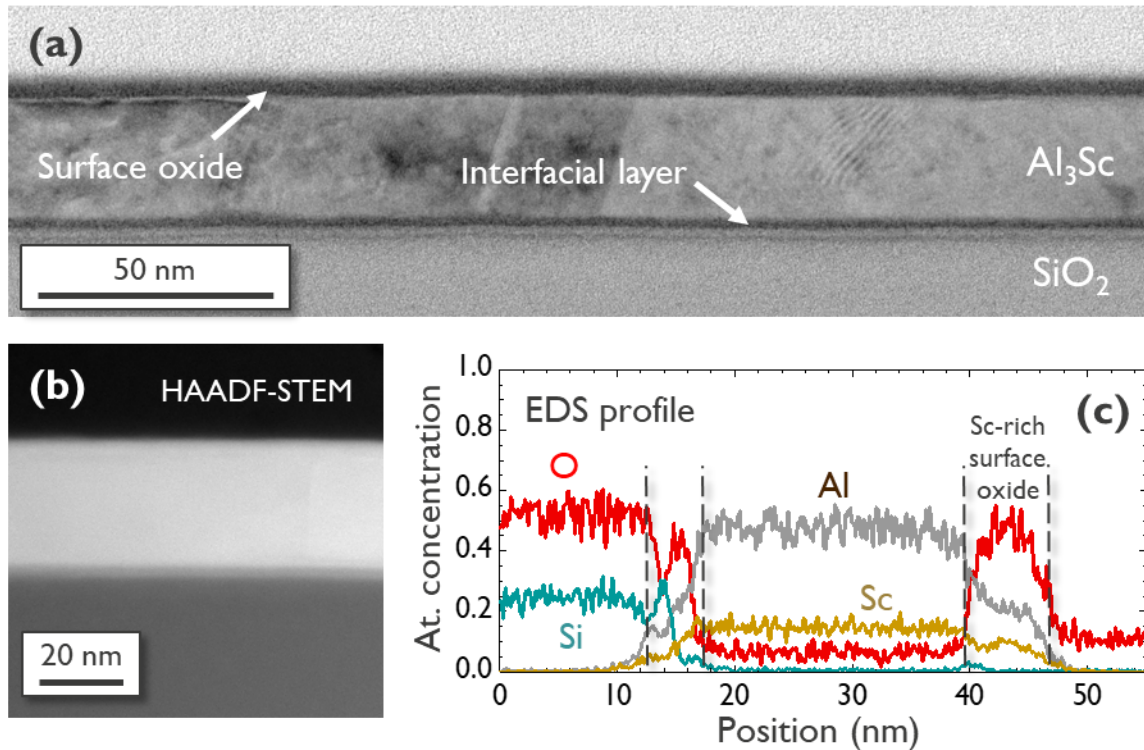

Figure 4. (a) Cross-sectional TEM image of an Al_3Sc film after annealing at 600°C. **(b)** High-angle annular dark field scanning TEM (HAADF-STEM) image of the Al_3Sc film. **(c)** Composition profile across the Al_3Sc film obtained by energy-dispersive spectroscopy (EDS).

CONCLUSION

We have reported the properties of Al_xSc_{1-x} thin films with compositions around Al_3Sc (x = 0.75) for potential interconnect metallization applications. As-deposited films were x-ray amorphous and (re-)crystallized above about 450°C, with an associated strong reduction of the resistivity. After annealing at 500°C, 24 nm thick Al_3Sc showed a resistivity of 12.6 μΩcm, considerably lower than previously reported values of NiAl, the so far most studied aluminide intermetallic for interconnect applications.[23-25] Further thickness scaling will rely on the limitation of non-stoichiometric native surface oxide formation that can affect the stoichiometry of ultrathin films.

ACKNOWLEDGEMENTS

This work was supported by imec's industrial affiliate program on nano-interconnects. The authors would like to thank Patrick Carolan, Hugo Bender, Kris Paulussen, Pieter Lagrain, Olivier Richard, Paola Favia, and Laura Nelissen for the TEM analysis; Inge Vaesen and Thierry Conard for the XPS profile; and the imec p-line for their support.

CREDIT AUTHORSHIP CONTRIBUTION STATEMENT

J-Ph. Soulié: Conceptualization, Methodology, Formal analysis, Investigation, Writing - Original Draft, Writing - Review & Editing. **K. Sankaran**: Conceptualization, Methodology, Software, Investigation, Writing - Review & Editing, Visualization. **V. Founta**: Conceptualization, Formal analysis, Investigation, Writing - Review & Editing. **K. Opsomer**: Methodology, Investigation, Writing - Review & Editing. **C. Detavernier**: Methodology, Investigation, Resources, Writing - Review & Editing, Supervision. **J. Van de Vondel**: Methodology, Validation, Writing - Review & Editing, Supervision. **G. Pourtois**: Methodology, Software, Validation, Resources, Writing - Review & Editing, Visualization. **Z. Tőkei**: Conceptualization, Methodology, Resources, Writing - Review & Editing, Project administration, Funding acquisition. **J. Swerts**: Conceptualization, Methodology, Resources, Writing - Review & Editing, Funding acquisition. **C. Adelmann**: Conceptualization, Methodology, Validation, Formal analysis, Writing - Original Draft, Writing - Review & Editing, Supervision.

REFERENCES

[1] P. Kapur, J.P. McVittie, and K.C. Saraswat, “Technology and reliability constrained future copper interconnects. I. Resistance modeling,” IEEE Trans. Electron Dev. **49**(4), 590–597 (2002), doi: 10.1109/16.992867

[2] D. Josell, S.H. Brongersma, and Z. Tőkei, “Size-dependent resistivity in nanoscale interconnects,” Ann. Rev. Mater. Res. **39**(1), 231–254 (2009), doi: 10.1146/annurev-matsci-082908-145415

[3] M.R. Baklanov, C. Adelmann, L. Zhao, and S. De Gendt, “Advanced interconnects: materials, processing, and reliability,” ECS J. Solid State Sci. Technol. **4**(1), Y1–Y4 (2014), doi: 10.1149/2.0271501jss

[4] D. Gall, “The resistivity bottleneck: the search for new interconnect metals,” 2020 Intern. Symp. VLSI Technol. Sys. App. (VLSI-TSA), 112–113 (2020), doi: 10.1109/VLSI-TSA48913.2020.9203700

[5] D. Gall, “Electron mean free path in elemental metals,” J. Appl. Phys. **119**, 085101 (2016), doi: 10.1063/1.4942216

[6] A.F. Mayadas and M. Shatzkes, “Electrical-resistivity model for polycrystalline films: the case of arbitrary reflection at external surfaces,” Phys. Rev. B **1**(4), 1382–1389 (1970), doi: 10.1103/PhysRevB.1.1382

[7] C. Adelmann, L.G. Wen, A.P. Peter, Y.K. Siew, K. Croes, J. Swerts, M. Popovici, K. Sankaran, G. Pourtois, S. Van Elshocht, J. Bömmels, and Z. Tőkei, “Alternative metals for advanced interconnects,” 2014 IEEE Intern. Interconnect Technol. Conf. (IITC), 173–176 (2014), doi: 10.1109/IITC.2014.6831863

[8] C. Adelmann, K. Sankaran, S. Dutta, A. Gupta, S. Kundu, G. Jamieson, K. Moors, N. Pinna, I. Ciofi, S. Van Eishocht, J. Bömmels, G. Boccardi, C.J. Wilson, G. Pourtois, and Z. Tőkei, “Alternative metals: from *ab initio* screening to calibrated narrow line models,” 2018 IEEE Intern. Interconnect Technol. Conf. (IITC), 154–156 (2018), doi: 10.1109/IITC.2018.8456484

[9] J. Kelly, J.H.- Chen, H. Huang, C.K. Hu, E. Liniger, R. Patlolla, B. Peethala, P. Adusumilli, H. Shobha, T. Nogami, T. Spooner, E. Huang, D. Edelstein, D. Canaperi, V. Kamineni, F. Mont, and S. Siddiqui, “Experimental study of nanoscale Co damascene BEOL interconnect structures,” 2016 IEEE Intern. Interconnect Technol. Conf. (IITC), 40–42 (2016), doi: 10.1109/IITC-AMC.2016.7507673

[10] S. Dutta, S. Beyne, A. Gupta, S. Kundu, S. Van Elshocht, H. Bender, G. Jamieson, W. Vandervorst, J. Bömmels, C.J. Wilson, Z. Tőkei, and C. Adelmann, “Sub-100 nm^2 cobalt interconnects,” IEEE Electron Dev. Lett. **39**(5), 731–734 (2018), doi: 10.1109/LED.2018.2821923

[11] C. Auth, A. Aliyarukunju, M. Asoro, D. Bergstrom, V. Bhagwat, J. Birdsall, N. Bisnik, M. Buehler, V. Chikarmane, G. Ding, Q. Fu, H. Gomez, W. Han, D. Hanken, M. Haran, M. Hattendorf, R. Heussner, H. Hiramatsu, B. Ho, S. Jaloviar, I. Jin, S. Joshi, S. Kirby, S. Kosaraju, H. Kothari, G. Leatherman, K. Lee, J. Leib, A. Madhavan, K. Marla, H. Meyer, T. Mule, C. Parker, S. Parthasarathy, C. Pelto, L. Pipes, I. Post, M. Prince, A. Rahman, S. Rajamani, A. Saha, J.D. Santos, M. Sharma, V. Sharma, J. Shin, P. Sinha, P. Smith, M. Sprinkle, A.S. Amour, C. Staus, R. Suri, D. Towner, A. Tripathi, A. Tura, C. Ward, and A. Yeoh, “A 10 nm high performance and low-power CMOS technology featuring 3rd generation FinFET transistors, self-aligned quad patterning,

contact over active gate and cobalt local interconnects," 2017 IEEE Intern. Electron Dev. Meet. (IEDM), 29.1.1-29.1.4 (2017), doi: 10.1109/IEDM.2017.8268472

[12] S. Dutta, K. Sankaran, K. Moors, G. Pourtois, S. Van Elshocht, J. Bömmels, W. Vandervorst, Z. Tőkei, and C. Adelmann, "Thickness dependence of the resistivity of platinum-group metal thin films," J. Appl. Phys. **122**, 025107 (2017), doi: 10.1063/1.4992089

[13] L.G. Wen, P. Roussel, O.V. Pedreira, B. Briggs, B. Groven, S. Dutta, M.I. Popovici, N. Heylen, I. Ciofi, K. Vanstreels, F.W. Østerberg, O. Hansen, D.H. Petersen, K. Opsomer, C. Detavernier, C.J. Wilson, S. Van Elshocht, K. Croes, J. Bömmels, Z. Tőkei, and C. Adelmann, "Atomic layer deposition of ruthenium with TiN interface for sub-10 nm advanced interconnects beyond copper," ACS Appl. Mater. Interfaces **8**(39), 26119–26125 (2016), doi: 10.1021/acsami.6b07181

[14] X. Zhang, H. Huang, R. Patlolla, W. Wang, F.W. Mont, J. Li, C.-K. Hu, E.G. Liniger, P.S. McLaughlin, C. Labelle, E.T. Ryan, D. Canaperi, T. Spooner, G. Bonilla, and D. Edelstein, "Ruthenium interconnect resistivity and reliability at 48 nm pitch," 2016 IEEE Intern. Interconnect Technol. Conf. (IITC), 31–33 (2016), doi: 10.1109/IITC-AMC.2016.7507650

[15] S. Dutta, K. Moors, M. Vandemaele, and C. Adelmann, "Finite size effects in highly scaled ruthenium interconnects," IEEE Electron Dev. Lett. **39**(2), 268–271 (2018), doi: 10.1109/LED.2017.2788889

[16] D. Tierno, M. Hosseini, M. van der Veen, A. Dangol, K. Croes, S. Demuynck, Z. Tőkei, E.D. Litta, and N. Horiguchi, "Reliability of barrierless PVD Mo," 2021 IEEE Intern. Interconnect Technol. Conf. (IITC), 1–3 (2021), doi: 10.1109/IITC51362.2021.9537545

[17] K. Sankaran, K. Moors, Z. Tőkei, C. Adelmann, and G. Pourtois, "*Ab initio* screening of metallic MAX ceramics for advanced interconnect applications," Phys. Rev. Mater. **5**, 056002 (2021), doi: 10.1103/PhysRevMaterials.5.056002

[18] S. Kumar, C. Multunas, B. Defay, D. Gall, and R. Sundararaman, "Ultralow electron-surface scattering in nanoscale metals leveraging Fermi-surface anisotropy," Phys. Rev. Mater. **6**, 085002 (2022), doi: 10.1103/PhysRevMaterials.6.085002

[19] J.H. Moon, E. Jeong, S. Kim, T. Kim, E. Oh, K. Lee, H. Han, and Y.K. Kim, "Materials quest for advanced interconnect metallization in integrated circuits," Adv. Sci. **10**(23), 2207321 (2023), doi: 10.1002/advs.202207321

[20] J. Koike, T. Kuge, L. Chen, and M. Yahagi, "Intermetallic compounds for interconnect metal beyond 3 nm node," 2021 IEEE Intern. Interconnect Technol. Conf. (IITC), 1–3 (2021), doi: 10.1109/IITC51362.2021.9537364

[21] L. Chen, D. Ando, Y. Sutou, and J. Koike, "$CuAl_2$ thin films as a low-resistivity interconnect material for advanced semiconductor devices," J. Vac. Sc. Technol. B **37**, 031215 (2019), doi: 10.1116/1.5094404

[22] J.-P. Soulié, Z. Tőkei, J. Swerts, and C. Adelmann, "Aluminide intermetallics for advanced interconnect metallization: thin film studies," 2021 IEEE Intern. Interconnect Technol. Conf. (IITC), 1–3 (2021), doi: 10.1109/IITC51362.2021.9537441

[23] L. Chen, D. Ando, Y. Sutou, D. Gall, and J. Koike, "NiAl as a potential material for liner- and barrier-free interconnect in ultrasmall technology node," Appl. Phys. Lett. **113**, 183503 (2018), doi: 10.1063/1.5049620

[24] L. Chen, D. Ando, Y. Sutou, S. Yokogawa, and J. Koike, "Liner- and barrier-free NiAl metallization: a perspective from TDDB reliability and interface status," Appl. Surf. Sci. **497**, 143810 (2019), doi: 10.1016/j.apsusc.2019.143810

[25] J.-P. Soulié, Z. Tőkei, J. Swerts, and C. Adelmann, "Thickness scaling of NiAl thin films for alternative interconnect metallization," 2020 IEEE Intern. Interconnect Technol. Conf. (IITC), 151–153 (2020), doi: 10.1109/IITC47697.2020.9515638

[26] J.B. Dunlop, G. Gruner, and A.D. Caplin, "Dilute intermetallic compounds. II. Properties of aluminium rich aluminium-transition metal phases," J. Phys. F: Met. Phys. **4**(12), 2203–2217 (1974), doi: 10.1088/0305-4608/4/12/016

[27] J.L. Murray, "The Al-Sc (aluminum-scandium) system," JPE **19**(4), 380–384 (1998), doi: 10.1361/105497198770342120

[28] P. Giannozzi, S. Baroni, N. Bonini, M. Calandra, R. Car, C. Cavazzoni, D. Ceresoli, G.L. Chiarotti, M. Cococcioni, I. Dabo, A.D. Corso, S. de Gironcoli, S. Fabris, G. Fratesi, R. Gebauer, U. Gerstmann, C. Gougoussis, A. Kokalj, M. Lazzeri, L. Martin-Samos, N. Marzari, F. Mauri, R. Mazzarello, S. Paolini, A. Pasquarello, L. Paulatto, C. Sbraccia, S. Scandolo, G. Sclauzero, A.P. Seitsonen, A. Smogunov, P. Umari, and R.M. Wentzcovitch, "QUANTUM ESPRESSO: a modular and open-source software project for quantum simulations of materials," J. Phys.: Condens. Matter **21**, 395502 (2009), doi: 10.1088/0953-8984/21/39/395502

[29] K.F. Garrity, J.W. Bennett, K.M. Rabe, and D. Vanderbilt, "Pseudopotentials for high-throughput DFT calculations," Comput. Mater. Sci. **81**, 446–452 (2014), doi: 10.1016/j.commatsci.2013.08.053

[30] J.P. Perdew, K. Burke, and M. Ernzerhof, "Generalized gradient approximation made simple," Phys. Rev. Lett. **77**(18), 3865–3868 (1996), doi: 10.1103/PhysRevLett.77.3865

[31] H.J. Monkhorst, and J.D. Pack, "Special points for Brillouin-zone integrations," Phys. Rev. B **13**(12), 5188–5192 (1976), doi: 10.1103/PhysRevB.13.5188

[32] K. Moors, K. Sankaran, G. Pourtois, and C. Adelmann, "First-principles-based screening method for resistivity scaling of anisotropic metals," Phys. Rev. Mater. **6**, 123804 (2022), doi: 10.1103/PhysRevMaterials.6.123804

[33] A. Gupta, B.T. Kavakbasi, B. Dutta, B. Grabowski, M. Peterlechner, T. Hickel, S.V. Divinski, G. Wilde, and J. Neugebauer, "Low-temperature features in the heat capacity of unary metals and intermetallics for the example of bulk aluminum and Al_3Sc," Phys. Rev. B **95**, 094307 (2017), doi: 10.1103/PhysRevB.95.094307

[34] G.R. Caskey, J.M. Franz, and D.J. Sellmyer, "Electronic and magnetic states in metallic compound—II: Electron transport and magnetic susceptibility in NiAl and FeAl," J. Phys. Chem. Sol. **34**(7), 1179–1198 (1973), doi: 10.1016/S0022-3697(73)80208-2